Sensors and Materials, Vol. 34, No. 12 (2022) 4787–4799
MYU Tokyo

S & M 3143

Feasibility of Terrestrial Laser Scanning System for Detecting and Monitoring Surface Displacement of Artificial Slopes on Forest Roads

Ikhyun Kim,[1†] Jeongjae Kim,[1†] Heesung Woo,[2] and Byoungkoo Choi[3*]

[1]Department of Forestry and Environmental Systems, Kangwon National University, Chuncheon 24341, Korea
[2]College of Forest and Environmental Sciences, Kangwon National University, Chuncheon 24341, Korea
[3]Division of Forest Sciences, Kangwon National University, Chuncheon 24341, Korea

(Received April 22, 2022; accepted August 24, 2022; online published September 12, 2022)

Keywords: forest road cut slope, terrestrial laser scanning system, iterative closest point, soil displacement measurement, grid method, digital evaluation model of difference

The steep gradient of artificial slopes on forest roads reduces the natural survival rate of vegetation. Uncovered vegetation slopes are exposed, resulting in soil displacement including soil erosion and sedimentation. Therefore, it is necessary to establish an optimized slope management plan with high accuracy for quantifying or detecting the erosion and deposition of artificial slopes. In this context, we investigated the possibility of using a terrestrial laser scanning system (TLS) to estimate soil displacement activity on a cut slope on a forest road. The soil displacement was estimated using time series point cloud data captured by a TLS. The differences among the captured point cloud data were calculated using a digital evaluation model of difference methodology. To validate the performance of the TLS for soil displacement estimation, 10 soil displacement markers were installed in a cut slope. The study revealed that the TLS detected the differences in soil erosion and deposition activity on an area of a steep slope. The differences in soil erosion and the depth of soil sediment were estimated to be 1.36 and 0.3 cm, respectively. The results of this research indicate the feasibility of using a TLS to investigate the surface displacement on a slope area, despite the errors of the estimated erosion and deposition.

1. Introduction

The forest road network is very important in forest activities including forest management, timber harvesting, regeneration, and protection.[1,2] However, artificial slopes on forest roads have several problems such as soil erosion and sedimentation.[3–5] Several factors affect soil erosion on a steep slope, including vegetation cover,[6,7] the gradient of the slope,[8,9] the intensity of precipitation,[7,10] and the soil texture.[11–13] In addition, the soil erosion and sedimentation on slopes are a major concern in water drainage management of forest roads. However, the vegetation survival and growth rates in steep slopes are limited due to the unstable soil condition

*Corresponding author: e-mail: bkchoi@kangwon.ac.kr
†These authors contributed equally to this work.
https://doi.org/10.18494/SAM3949

ISSN 0914-4935
https://myukk.org/

and soil run-off.[14–17] For these reasons, several studies have been conducted to investigate efficient ways to monitor forest road displacement activity using field-based and remote sensing techniques.

In general, soil erosion and displacement on slopes are evaluated by field-based methods including leveling and the installation of sensors to detect soil movement.[18] However, conservative methods such as leveling are insufficient for the quantitative and accurate evaluation of slope displacement.[19] In addition, monitoring sensors are expensive to install, require continuous maintenance, and cannot guarantee data continuity.

Recently, laser or light detection and ranging (LiDAR) scanning systems have been used to detect soil surface displacement.[20–24] Several laser scanning systems for different types of applications exist. Terrestrial-fixed, terrestrial-mobile, and airborne systems are classified by the types of platforms to which they are applied. In forestry, airborne systems employing lasers are mostly used because of their ability to cover large areas. However, airborne systems have limited ability to detect the under-canopy inventory due to the high density of the canopy layer, which includes crowns and tree leaves. To overcome these limitations, terrestrial laser scanning systems (TLSs) are used to gather under-canopy point cloud data (PCD). The primary advantage of using a TLS is the ability to obtain high-intensity PCD in the under-canopy area. A TLS application provides precise 3D PCD for detecting the ground surface, making it suitable for activities such as soil displacement and erosion monitoring.[25–28]

In general, cross-sectional, triangular prism, grid, and digital evaluation model (DEM) of difference (DoD) methodologies are used to estimate surface displacement.[29–33] A cross-sectional methodology is mainly used in landslide surveys.[31,32] The triangular prism method is the most accurate volume estimation method,[31–33] but it is difficult to accurately detect elevation changes. The DoD methodology is commonly adopted to estimate the vertical difference (VD) between two sets of time series data with high spatial resolution.[29,30] In addition, the grid methodology is widely used to estimate the volume of surface displacement.[31–33]

In this background, in this study we investigated the possibility of estimating the surface displacement of a slope on a forest road using a TLS-based digital terrain model (DTM). We estimated the VD by applying the DoD methodology. In addition, the volume of the displacement was estimated using the grid methodology. The results of this study will provide valuable information for the future application of 3D scanning systems by forest researchers and managers interested in cost- and labor-efficient forest road management.

2. Materials and Methods

2.1 Overview

A flow chart of the overall research procedure is presented in Fig. 1. Time series PCD were acquired at research sites, and the collected PCD were processed. Then co-registration of paired PCD was conducted using the iterative closet point (ICP) algorithm. We used the DoD method to calculate the change between the June 2021 and August 2021 PCD and quantify the areas of

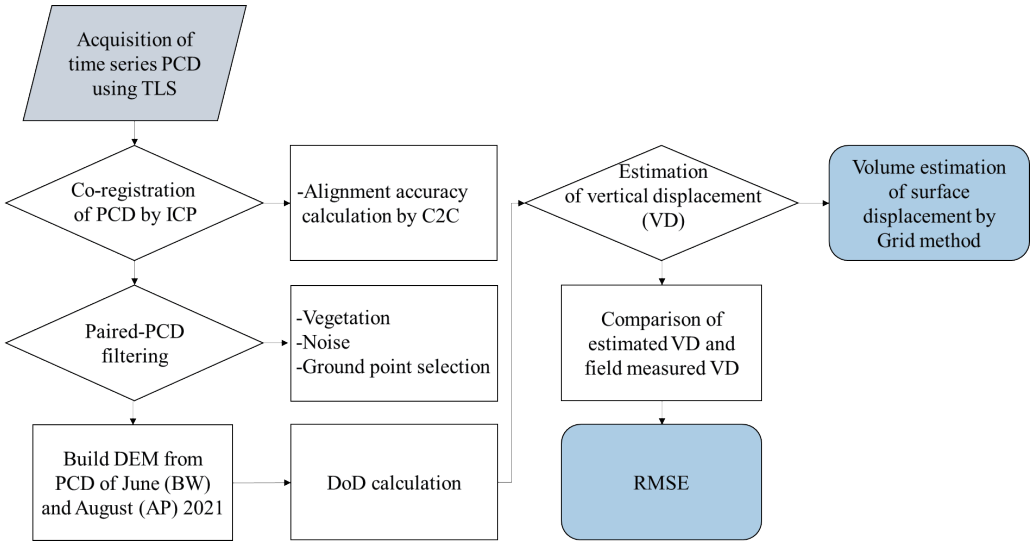

Fig. 1. (Color online) Overall procedure of estimation of VD using TLS.

erosion and deposition.[34] The estimated depth was validated by comparison with field-measured ground truth data at checkpoints (CHKs).

2.2 Site description

The research site was located in the research forest of Kangwon National University, Bongmyeong, Chuncheon, Gangwon, South Korea (37°46'07.3"N, 127°50'50.2"E) (Fig. 2). The average soil bulk density on the slope surface (0–10 cm soil depth) was recorded as 1.32 g/cm^3. The gradient of the forest road was approximately 17.81° and the gradient of the artificial cut slope was approximately 40.87°.

The average annual precipitation and temperature over 30 years (1992–2021) were 1319.59 mm and 10.90 °C, respectively. The cut slope on the forest road had been constructed with a 1-m-high retaining wall to prevent sedimentation. The wet season of South Korea (Jangma) generally begins in June or early July and lasts 2–6 weeks. The daily average precipitation in the research period (from June 20 to August 6, 2021) was 5 mm and the total precipitation recorded was 240.2 mm. The daily average temperature during the study period was 25.62 °C at Hongcheon weather station, 11 km from the study site.

2.3 Field survey and PCD acquisition

We used a Leica BLK360 imaging laser scanner (Leica Geosystems, Heerbrugg, Switzerland) for the terrestrial laser system. The weight of the scanner is 1 kg and the system can collect a 300° × 360° field of view. The system only records the first return of the laser pulse. The capacity of the battery of the scanner is sufficient for one day of scanning and exporting data. The scanner can scan an object with a capture speed of 360000 points/s, providing 300° (vertical) × 360° (horizontal) detection with a radius of 60 m and an accuracy of ±6 mm at

Fig. 2. (Color online) (a) Location of study site in experimental forest of Kangwon National University and (b) panoramic view of cut slope on forest road.

10 m. As the distance between the scanner and the object increases, the accuracy slightly decreases. At 20 m, the accuracy is 8 mm. In this study, the BLK360 scanner was utilized as the TLS for the VD detection and measurement of the cut slope. The study period consisted of two days: one before the wet season (BW; June 20, 2021) and one after the intensive precipitation period (AP; August 6, 2021), during which the VD of the slope on the forest road was investigated to examine the impact of intensive precipitation on the slope surface. The 3D scanning PCD were acquired in the same position by marking scanning spots in BW and AP (Fig. 3).

To detect the VD between two sets of time series data, a total of 10 CHKs were installed on profile AB in Fig. 4, and the VD was measured at each point to validate the VD estimated using the TLS. A polyvinyl chloride (PVC) pipe with inner diameter of 2.6 cm and outer diameter of 2.0 cm was installed on the slope to mark the location of the CHKs (Fig. 4). A ruler with mm resolution in the range of 0–50 cm was attached to the PVC pipe to measure changes in the VD. The ground truth data were recorded simultaneously with the collection of 3D scanning data. The VD on the slope was then calculated through the difference in surface height between BW and AP, which was used as ground-measured truth data.

2.4 Data processing

The data acquired using the TLS were converted into PCD format using Autodesk ReCap ver. 2021 (Autodesk ReCap, 2021). Co-registration of the time series PCD is essential for measuring morphological changes.[35,36] Since there was no spatial information in the 3D PCD, the ICP algorithm was adopted in this study. This algorithm statistically minimizes errors in the process of the co-registration of sets of PCD (Fig. 5).[37] The ICP algorithm uses a stable reference PCD, which is $p_i \in P$, to determine changes in the target PCD, which is $q_i \in Q$; the rotation R and translation t between p_i and q_i are calculated using the following error function formula:[22,37,38]

(a) (b) (c)

Fig. 3. (Color online) (a) BLK360 scanner used as TLS to detect VD of cut slope of forest road, (b) BLK360 scanner installed at edge of forest road, and (c) two measurements conducted at same point by marking installation point with piles.

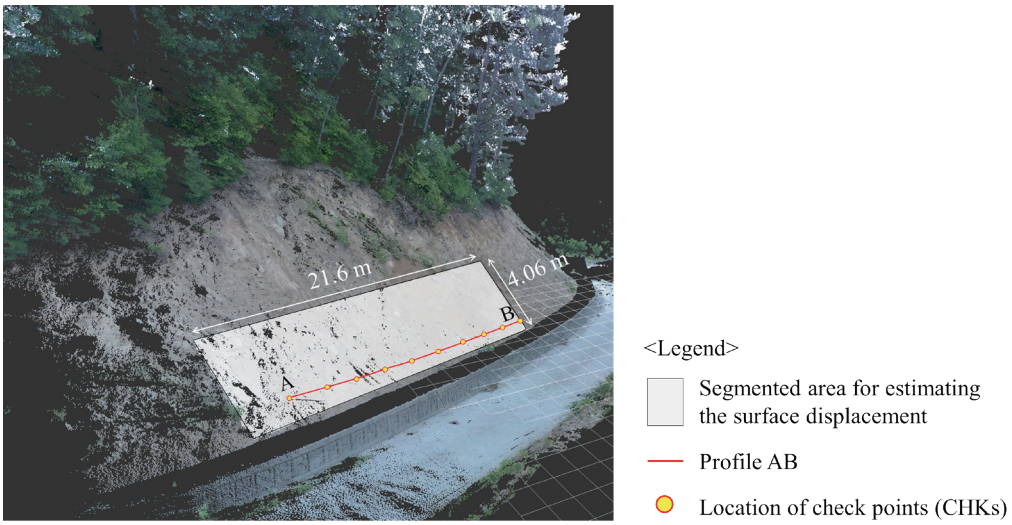

Fig. 4. (Color online) CHK installation points for measuring surface height on slope, and profile AB showing locations of CHKs. The rectangle represents the target area for estimating the VD.

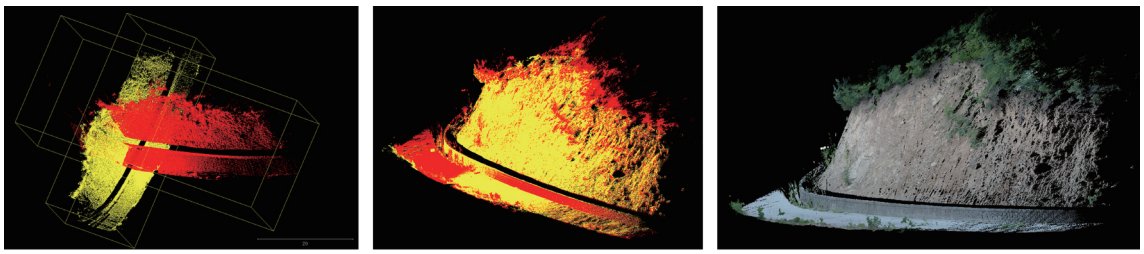

(a) (b) (c)

Fig. 5. (Color online) Process of co-registration of two time series of PCD using ICP algorithm. (a) Two time series of PCD before co-registration. The yellow PCD was acquired in BW, and the red PCD was acquired in AP. (b) Co-registration completed using ICP algorithm with the two sets of PCD overlapped. (c) RGB applied to co-registered PCD.

$$E(R,t) = \min_{R,t} \sum_i || a_i - (Rq_i + -t) ||^2 \quad (1)$$

Here, $p_i \in P$ = a point from 3D reference PCD and $q_i \in Q$ = a point from target PCD.

Paired PCD sets were co-registered using the ICP algorithm with a root mean square (RMS) difference of 0.00001, 20 iterations, and the final overlap set to 100%. CloudCompare software was used to perform the ICP algorithm (CloudCompare ver. 2.12 alpha). For accuracy validation of the co-registration alignment, the cloud-to-cloud (C2C) distance was computed with a set octree of level 10.

The paired DTM was constructed using the paired PCD to estimate the VD of the slope. Vegetation was filtered in CloudCompare (ver. 2.12 alpha) using the cloth simulation filter (CSF) tool. CSF is a classification algorithm that extracts ground points in discrete return PCD sets. The set parameter values were a cloth resolution of 0.1, a maximum of 500 iterations, and a classification threshold of 0.5.

2.5 Assessment of VD on slope surface

DoD was calculated using ArcGIS 10.8 to estimate the VD of the slope surface. All vertically altered points from DoD were identified as erosion (positive values) or sedimentation (negative values). Then, the erosion and sedimentation areas were reclassified for mapping. Lastly, the ratio of the areas was calculated. The total volume and the erosion and sedimentation areas were estimated using the grid method.

The accuracy of the estimated VD of the CHKs was compared with the ground truth data (the field-measured height of the surface) at the same location. The PCD of the CHKs were manually segmented. The estimated VD was analyzed using MATLAB R2019B (9.7.0.1190202). Additionally, the accuracy was validated using the root mean square error (RMSE) and bias respectively defined as

$$RMSE = \sqrt{\frac{\sum(\hat{x}_i - x_i)^2}{n}}, \quad (1)$$

$$bias = \frac{1}{n}\sum_{i=1}^{n}(\hat{x}_i - x_i), \quad (2)$$

where n is the number of estimates, $\hat{x}_i$ is the estimated VD of the CHKs, and x_i is the field-measured ground truth data. Data were analyzed using R statistics (R Core Team, 2021). The data were processed and analyzed using an AMD Ryzen 5 3500 CPU 64-bit system (3.60 GHz, RTX 3060 Nvidia GPU, 64.0 GB RAM).

3. Results

3.1 Results of data processing

As shown in Table 1, the total processing time was approximately 54 min. Field data collection using the BLK360 scanner took 14 min including the installation of the scanner on the scanning spot. Filtering using the CSF took 5 min, and the generation of DTMs required 20 s. The negative and positive values from DoD corresponded to the sedimentation and erosion areas, respectively. These areas were reclassified for the VD map. Additionally, the processing time for area measurements and reclassifications took 10 min, and the volumetric estimation took 10 min.

The DTMs for BW and AP, which were filtered from the respective PCD, visibly depict rill erosion (Fig. 6). Both DTMs are built with fine resolution (7.09 and 6.93 mm/pix, respectively) (Table 2). Several prior studies used the TLS-based DEM with 1–20 cm grid size to investigate rill erosion.[39–41]

As a result of the co-registration of the two time series PCD (BW and AP) using the ICP algorithm, we obtained a C2C distance and standard deviation of 2.4 and 2.1 cm, respectively,

Table 1
Time requirement for each data acquisition process and entire process.

		Processing time
PCD acquisition from TLS	3D scanning	14 (7 × 2) min
	PCD formation	6 (3 × 2) min
Co-registration of two time series of PCD		3 min
Filtering using CSF		5 (2.5 × 2) min
Generation of DTMs		20 (10 × 2) s
DoD		5 min
Estimation of VD	Area	10 min
	Volume	10 min
Total process		54 min 20 s

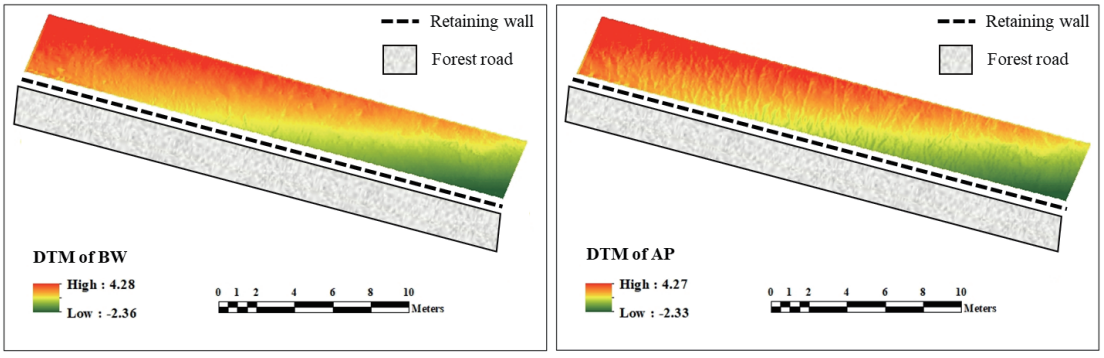

(a) (b)

Fig. 6. (Color online) DTMs for (a) BW and (b) AP.

Table 2
Statistical results of 3D data acquisition and co-registration accuracy.

	BW	AP
Raw PCD	24246384	24241190
Filtered PCD from raw PCD	13129484	12759979
Segmented PCD for DTM	4349211	4311089
DTM resolution (mm/pix)	7.09	6.93
Total DoD area[a] (m^2)	68.0	
Outlier-removed DoD area (m^2)	66.01	
C2C distance (cm)	2.4	
RMS[b] (cm)	16.3	
S.D.[c] (cm)	2.1	

[a]length of forest road 3D scanning data
[b]RMS between two sets of 3D scanning data
[c]standard deviation

and the RMS was approximately 16.3 cm (Table 2). Sulzer *et al.*[42] reported that the median values of the vertical C2C of PCD sets based on a TLS were –3 to –3.05 cm relative to the GNSS control points. In addition, Ruggles *et al.*[43] observed that the median C2C values of PCD co-registration using the ICP algorithm were approximately 3.3, 13.8, and 13.7 cm different from the TLS ground model for three platforms. RMS values of PCD co-registration using the ICP algorithm have been reported to range from 4 to 25 cm.[44,45] After co-registration, the areas to be analyzed were selected from each raw PCD set, and the two selected areas were approximately 87.7 m^2. To determine the morphological changes, bare-soil areas were selected for the DTMs; the numbers of selected ground points were 4,349,211 (BW) and 4,311,089 (AP) (Table 2).

3.2 Estimated VD in cut slope

DoD indicates that the segmented area in the cut slope resulted in negative and positive values, which were designated soil erosion and sedimentation areas, respectively. The total area for DoD was 66.01 m^2 after removing outliers due to co-registration errors (Table 3). The computed erosion and segmentation rates for the selected area were 74.27% (2196610 cm^3) and 25.72% (319044 cm^3), respectively (Table 3). Notably, the erosion area was 32.05 m^2 larger than the sedimentation area (Table 3). Moreover, the total erosion volume exceeded the total sedimentation volume by 1,877,566 cm^3 (Table 3). The area for DoD was 68 m^2 before filtering the outliers and 66.01 m^2 afterwards, while the segmented area in the cut slope was 87.7 m^2 (Tables 2 and 3).

The soil eroded by approximately 0–11 cm in the erosion areas and accumulated by approximately 0–11 cm in the sedimentation areas (Fig. 7). The erosion and sedimentation areas were automatically reclassified by ArcGIS software (Fig. 7). The sedimentation areas were mainly distributed on the right side of the slope based on DoD. In about 81% of the total sedimentation area, the soil was deposited to a depth of 0–3 cm (Fig. 7). Most of the erosion areas were separated from the sedimentation areas, except for those in which the soil was eroded to a depth of 0–3 cm (Fig. 7).

Table 3
Vertical difference in cut slope on forest road estimated from BW to AP.

DoD from BW to AP	Area (m^2)	Ratio (%)	Volume (cm^3)
Total	66.01	100	—
Erosion	49.03	74.27	2196610
Sedimentation	16.98	25.72	319044

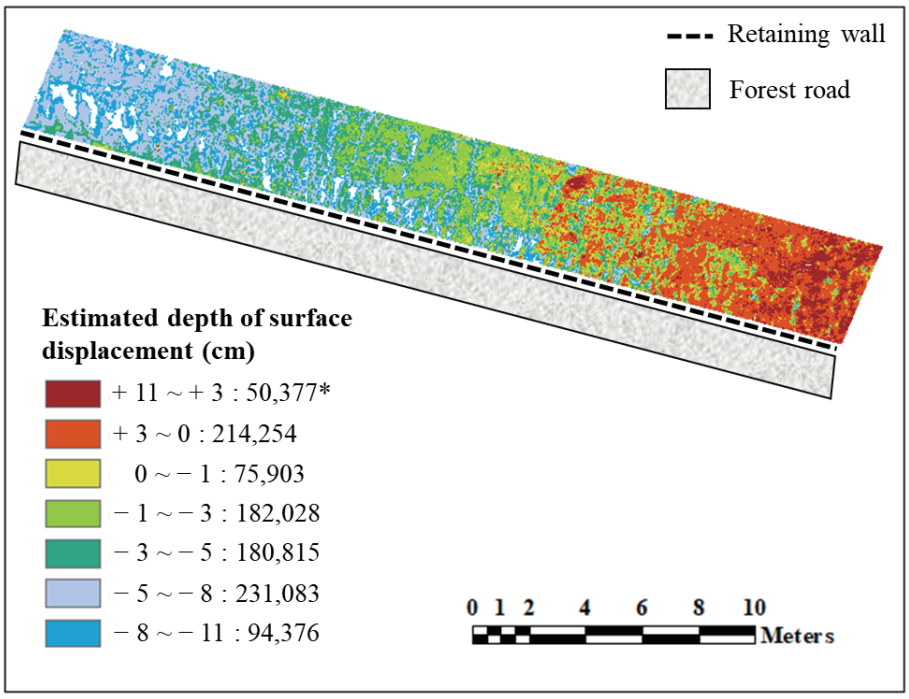

Fig. 7. (Color online) Results of reclassified DoD to identify erosion and sedimentation areas in cut slope. Negative and positive values represent depths of erosion and sedimentation, respectively. *Values after colons represent the number of DTM pixels corresponding to each class.

3.3 Validation of estimated VD at CHKs

The total VD depth, erosion depth, and sedimentation depth were estimated by subtracting the surface height values of the DTM of AP from those of the DTM of BW at the CHKs (Fig. 8, Table 4). As shown in Fig. 8, deposition occurred mainly at CHK Nos. 8, 9, and 10, which was the same result as that of DoD (Figs. 7 and 8). However, DoD includes potential errors caused by noise, registration error, and errors of the TLS.[34] The RMSE and bias between the ground-measured truth data and the estimated VD were 1.01 and 0.68, respectively (Table 4). The ground data and the estimated soil erosion depth differed by a factor of about 2.5 (Table 4).

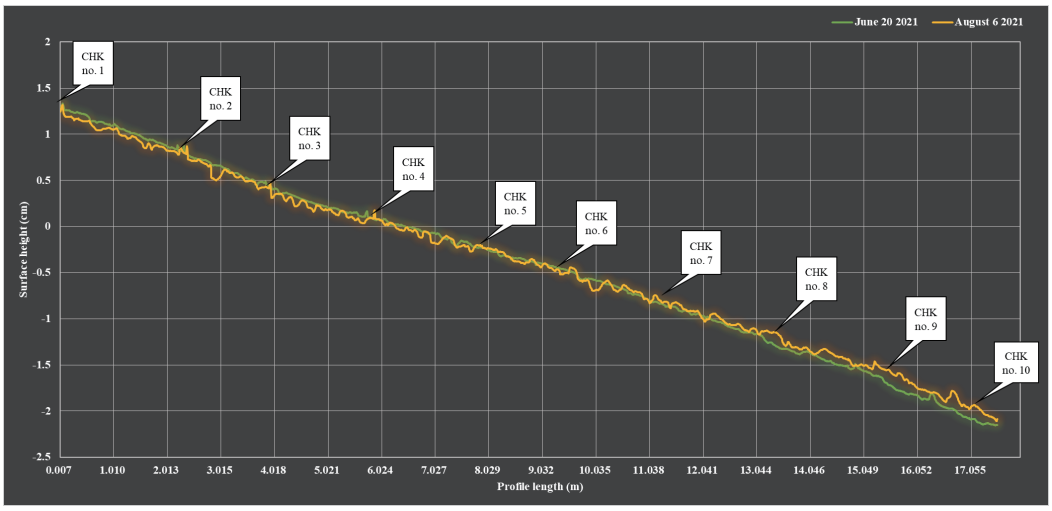

Fig. 8. (Color online) Estimated surface height from TLS along profile AB on BW and AP.

Table 4
Results of RMSE and bias between estimated VD and ground truth data of CHKs.

Data	VD				Erosion (cm)	Sedimentation (cm)
	Average (cm)	SE[a]	RMSE	Bias		
Reference (Ground data)	1.71	0.27	—	—	3.48	0.56
Estimated data (DoD)	1.03	0.25	1.01	0.68	1.36	0.3

[a]standard error

4. Discussion

The use of a LiDAR sensor is still a challenge in the practical assessment of VD in forests with high accuracy because of the co-registration of the time series PCD, and noise and outlier removal issues from the PCD. In addition, the validation of the estimated VD using ground-measured truth data is difficult. Nevertheless, successful alignments from raw PCD sets were realized in this study owing to the use of recognition points, such as the forest road and the retaining wall, as markers for the ICP process. However, morphological features, such as rough surfaces, may cause shadows, which can limit the accuracy of 3D detection using a TLS. The estimated area of 87.7 m^2 was underestimated as 68 m^2 due to distortion error.

In this study area, the total area of erosion in the forest road cut slope was about three times the total area of deposition, and the types of erosion were sheet erosion and rill erosion. However, scanning the rill erosion area from the side (the location of the 3D scanner) was insufficient to obtain the soil erosion depth. In fact, the ground-measured erosion depth was about 2.5 times the estimated erosion depth; thus, it is possible to detect eroded areas using ground-fixed LiDAR, but it appears to be difficult to accurately determine the erosion depth in centimeters. Despite issues relevant to the accuracy of estimating the VD on the cut slope, the results of this study were not only sufficient to distinguish between erosion and sedimentation but could also be used to evaluate where erosion occurred.

5. Conclusions

In this study, TLS data were used to calculate the approximate volumes of erosion and sedimentation on the cut slope of a forest road, which was found to be a more objective method than the conventional method. In addition, it was possible to distinguish between erosion and sedimentation areas on the slope using a TLS. However, the VD validation process was only conducted at CHKs. Also, the lack of a validation process in overall target areas and the C2C difference (2.4 cm) indicated that the errors that occurred may have been generated from the equipment system, limitations of sensors, and data collection and processing phases. Nevertheless, despite some limitations and errors of LiDAR application in soil displacement detection, the results of this research indicate the feasibility of using a TLS to investigate the surface displacement on a slope area.

Acknowledgments

This study was carried out with the support of the R&D Program for Forest Science Technology (Project No. 2021367B10–2223-BD01) commissioned by Korea Forest Service (Korea Forestry Promotion Institute).

References

1 Y. Miyamoto and H. Igarashi: (Sci. Bull. UNFU) Науковий вісник НЛТУ України. **14** (2004) 3.
2 S. Guamus, H. H. Acar, and D. Toksoy: Environ. Monit. Assess. **142** (2008) 1. https://doi.org/10.1007/s10661-007-9912-y
3 D. J. Holz, K. W. Williard, P. J. Edwards, and J. E. Schoonover: J. Contemp. Water Res. Educ. **154** (2015) 1. https://doi.org/10.1111/j.1936-704X.2015.03187.x
4 T. Varol, M. Ertuğrul, H. B. Özel, T. Emir, and M. Çetin: Appl. Ecol. Environ. Res. **17** (2019) 1. https://doi.org/10.15666/aeer/1701_825839
5 A. Srivastava, E. S. Brooks, M. Dobre, W. J. Elliot, J. Q. Wu, D. C. Flanagan, J. A. Gravelle, and T. E. Link: Sci. Total Environ. **701** (2020) 134877. https://doi.org/10.1016/j.scitotenv.2019.134877
6 X. Zhang, G. Q. Yu, Z. B. Li, and P. Li: Water Resour. Manage. **28** (2014) 9. https://doi.org/10.1007/s11269-014-0603-5
7 S. Stefanidis and D. Stathis: Water **10** (2018) 10. https://doi.org/10.3390/w10101469
8 B. Fu: Soil Use Manage. **5** (1989) 2. https://doi.org/10.1111/j.1475-2743.1989.tb00765.x
9 F. Turkelboom, J. Poesen, I. Ohler, K. Van Keer, S. Ongprasert, and K. Vlassak: Catena **29** (1997) 1. https://doi.org/10.1016/S0341-8162(96)00063-X
10 M. A. Nearing, V. Jetten, C. Baffaut, O. Cerdan, A. Couturier, M. Hernandez, Y. Le Bissonnais, M. H. Nichols, J. P. Nunes, C. S. Renschler, V. Souchère, and K. Van Oost: Catena **61** (2005) 2. https://doi.org/10.1016/j.catena.2005.03.007
11 A. I. Mamedov, G. J. Levy, I. Shainberg, and J. Letey: Soil Res. **39** (2001) 6. https://doi.org/10.1071/SR01029
12 J. Vahabi and D. Nikkami: Int. J. Sediment Res. **23** (2008) 4. https://doi.org/10.1016/S1001-6279(09)60008-1
13 M. Jourgholami and E. R. Labelle: Ann. For. Sci. **77** (2020) 1. https://doi.org/10.1007/s13595-020-00938-0
14 E. Bochet, P. García-Fayos, and J. Tormo: Land Degrad. Dev. **21** (2010) 2. https://doi.org/10.1002/ldr.911
15 J. W. Lee, C. M. Park, and H. Rhee: Land Degrad. Dev. **24** (2013) 6. https://doi.org/10.1002/ldr.2248
16 S. H. Kil, D. K. Lee, H. G. Kim, N. C. Kim, S. Im, and G. S. Park: Sustainability **7** (2015) 11. https://doi.org/10.3390/su71115319
17 X. Zhao, Z. Li, D. Zhu, Q. Zhu, M. D. Robeson, and J. Hu: Land Degrad. Dev. **29** (2018) 9. https://doi.org/10.1002/ldr.2988
18 V. T. Bickel, A. Manconi, and F. Amann: Remote Sens. **10** (2018) 6. https://doi.org/10.3390/rs10060865

19 S. Varbla, A. Ellmann, and R. Puust: Autom. Constr. **128** (2021) 103787. https://doi.org/10.1016/j.autcon.2021.103787
20 T. Stahl and A. Tye: Earth Surf. Process. Landforms **45** (2020) 2. https://doi.org/10.1002/esp.4748
21 W. Matwij, W. Gruszczyński, E. Puniach, and P. Ćwiąkała: Measurement **180** (2021) 109482. https://doi.org/10.1016/j.measurement.2021.109482
22 N. Ahmad Fuad, A. R. Yusoff, Z. Ismail, and Z. Majid: Int. Arch. Photogramm. Remote Sens. Spat. Inf. Sci. **42** (2018) 11. https://doi.org/10.5194/isprs-archives-XLII-4-W9-11-2018
23 R. Ossowski and P. Tysiąc: Pol. Marit. Res. **25** (2018) 140. https://doi.org/10.2478/pomr-2018-0065
24 S. Kalenjuk, W. Lienhart, and M. J. Rebhan: Comput.-Aided Civ. Infrastruct. Eng. **36** (2021) 6. https://doi.org/10.1111/mice.12656
25 M. J. Campbell, P. E. Dennison, A. T. Hudak, L. M. Parham, and B. W. Butler: Remote Sens. Environ. **215** (2018) 380. https://doi.org/10.1016/j.rse.2018.06.023
26 Y. Sun: Evaluating the Quality of Ground Surfaces Generated from Terrestrial Laser Scanning (TLS) Data (Doctoral dissertation, Virginia Tech) (2019). http://hdl.handle.net/10919/90577
27 S. Li, T. Wang, Z. Hou, Y. Gong, L. Feng, and J. Ge: Ecol. Indic. **121** (2021) 107011. https://doi.org/10.1016/j.ecolind.2020.107011
28 J. Novotny, B. Navratilova, J. Albert, E. Cienciala, L. Fajmon, and O. Brovkina: Remote Sens. Appl. Soc. Environ. **23** (2021) 100574. https://doi.org/10.1016/j.rsase.2021.100574
29 D. Lague, N. Brodu, and J. Leroux: ISPRS J. Photogramm. Remote Sens. **82** (2013) 10. https://doi.org/10.1016/j.isprsjprs.2013.04.009
30 Y. C. Hsieh, Y. C. Chan, and J. C. Hu: Remote Sens. **8** (2016) 3. https://doi.org/10.3390/rs8030199
31 G. Tucci, A. Gebbia, A. Conti, L. Fiorini, and C. Lubello: Remote Sens. **11** (2019) 12. https://doi.org/10.3390/rs11121471
32 F. H. Abulrahman: JUD **23** (2020) 1. https://doi.org/10.26682/sjuod.2020.23.1.2
33 M. Pepe, D. Costantino, V. S. Alfio, and N. Zannotti: Geogr. Tech. **16** (2021) 1. https://doi.org/10.21163/GT_2021.163.01
34 X. Lu, Y. Li, R. A. Washington-Allen, Y. Li, H. Li, and Q. Hu: Int. Soil Water Conserv. Res. **5** (2017) 3. http://dx.doi.org/10.1016/j.iswcr.2017.06.002
35 M. V. Peppa, J. P. Mills, P. Moore, P. E. Miller, and J. E. Chambers: Earth Surf. Process. Landforms **44** (2019) 1. https://doi.org/10.1002/esp.4502
36 S. Cucchiaro, E. Maset, M. Cavalli, S. Crema, L. Marchi, A. Beinat, and F. Cazorzi: GIsci. Remote Sens. **57** (2020) 5. https://doi.org/10.1080/15481603.2020.1763048
37 P. J. Besl and N. D. McKay: Sensor Fusion IV Control Paradigms and Data Structures **1611** (1992) 586. https://doi.org/10.1117/12.57955
38 B. Moghaddame-Jafari: Geoge Mason Univ. (2017). https://hdl.handle.net/1920/10810
39 G. Hancock, D. Crawter, S. Fityus, J. Chandler, and T. Wells: Earth Surf. Process. Landforms **33** (2008) 1006. https://doi.org/10.1002/esp.1585
40 A. Eltner and P. Baumgart: Geomorphology **245** (2015) 243. https://doi.org/10.1016/j.geomorph.2015.06.008
41 P. Zhang, H. Tang, W. Yao, N. Zhang, and L. Xizhi: Catena **137** (2016) 536. https://doi.org/10.1016/j.catena.2015.10.025
42 W. Sulzer, P. Lindbichler, G. Seier, and J. Gspurning: Acta Geobalcanica **8** (2021) 85. https://doi.org/10.18509/AGB218-30851
43 S. Ruggles, J. Clark, K. W. Franke, D. Wolfe, B. Reimschiissel, R. A. Martin, T. J. Okeson, and J. D. Hedengren: J. Unmanned Veh. Syst. **4** (2016) 4. https://doi.org/10.1139/juvs-2015-0043
44 C. Toth, D. Brzezinska, N. Csanyi, E. Paska, and N. Yastikli: Proc. 2007 ARPRS Annu. Conf. (ASPRS, 2007) 1–11.
45 E. Nissen, A. K. Krishnan, J. R. Arrowsmith, and S. Saripalli: Geophys. Res. Lett. **39** (2012) 16. https://doi.org/10.1029/2012GL052460

About the Authors

Ikhyun Kim received his B.S. and M.S. degrees from Kangwon National University, South Korea, in 2019 and 2021, respectively. Currently, he is a Ph.D. candidate at Kangwon National University, South Korea. His research interests include forest environment protection, forest soil, and forest engineering. (kih9281@kangwon.ac.kr)

Jeongjae Kim received his B.S. degree from Kangwon National University, South Korea, in 2021. Currently, he is an M.S. candidate at Kangwon National University, South Korea. His research interests include forest environment protection. (202116435@kangwon.ac.kr)

Heesung Woo received his B.S. degree from Kangwon National University, South Korea, in 2011, his first and second M.S. degrees from Kangwon National University, South Korea, in 2013 and Humboldt State University, CA, USA, in 2015, respectively, and his Ph.D. degree from the University of Tasmania, Australia, in 2020. From 2019 to 2020, he was a research professor at Kyungpook National University, South Korea. Since 2021, he has been a research professor at Kangwon National University. His research interests are in precision forestry, robotics in forestry, and data analysis in forest management. (whs1608@gmail.com)

Byoungkoo Choi received his B.S. and M.S. degrees from Kangwon National University, South Korea, in 2002 and 2004, respectively, and his Ph.D. degree from Mississippi State University, USA, in 2011. From 2014 to 2015, he was a research scientist at the National Institute of Ecology, South Korea. Since 2015, he has been an associate professor at Kangwon National University. His research interests include eco-hydrology, watershed management, and forestry BMPs. (bkchoi@kangwon.ac.kr)